*Published online 7 January 2009*

*Nucleic Acids Research, 2009, Vol. 37, No. 4* ***1107–1114***
*doi:10.1093/nar/gkn1011*

# Mechanism of DNA flexibility enhancement by HMGB proteins

**Jingyun Zhang[1], Micah J. McCauley[1], L. James Maher III[2], Mark C. Williams[1,3,*] and N. E. Israeloff[1,3,*]**

[1]Department of Physics, Northeastern University, Boston, MA 02115, [2]Department of Biochemistry and Molecular Biology, Mayo Clinic College of Medicine, Rochester, MN 55905 and [3]Center for Interdisciplinary Research on Complex Systems, Northeastern University, Boston, MA 02115, USA

Received October 21, 2008; Revised December 2, 2008; Accepted December 4, 2008

## ABSTRACT

**The mechanism by which sequence non-specific DNA-binding proteins enhance DNA flexibility is studied by examining complexes of double-stranded DNA with the high mobility group type B proteins HMGB2 (Box A) and HMGB1 (Box A+B) using atomic force microscopy. DNA end-to-end distances and local DNA bend angle distributions are analyzed for protein complexes deposited on a mica surface. For HMGB2 (Box A) binding we find a mean induced DNA bend angle of 78°, with a standard error of 1.3° and a SD of 23°, while HMGB1 (Box A+B) binding gives a mean bend angle of 67°, with a standard error of 1.3° and a SD of 21°. These results are consistent with analysis of the observed global persistence length changes derived from end-to-end distance measurements, and with results of DNA-stretching experiments. The moderately broad distributions of bend angles induced by both proteins are inconsistent with either a static kink model, or a purely flexible hinge model for DNA distortion by protein binding. Therefore, the mechanism by which HMGB proteins enhance the flexibility of DNA must differ from that of the *Escherichia coli* HU protein, which in previous studies showed a flat angle distribution consistent with a flexible hinge model.**

## INTRODUCTION

It is important to understand the effects of protein binding on DNA conformation in the context of DNA transcription and replication. The role of sequence non-specific DNA-binding proteins such as HMGB in these processes (1–4) and more generally in gene expression (4) is under intense investigation. Like *Escherichia coli* HU proteins, HMGB proteins have been shown to create bends and promote looping in DNA (5,6), which may facilitate transcription or repression. Double-stranded (ds) DNA is compacted when HMGB proteins are present, indicative of a reduced persistence length, $p$, and enhanced polymer flexibility (1). Two very different biophysical mechanisms have been proposed to account for protein-enhanced DNA flexibility. In the static kink model (5,6), transient protein-binding events produce fixed-angle bends in the DNA at the binding sites. In the flexible hinge model, protein binding is thought to enhance the flexibility of DNA in one plane, with no preferential angle at the binding site (7).

A static kink model is suggested by X-ray crystallography studies of sequence non-specific HMGB proteins, where estimates for the induced bending angle are 111.1° for single box HMGB protein binding (as measured for the *Drosophila melanogaster* HMG-D protein, which may differ from the HMGB proteins studied here) (8) and $101.5° \pm 9.1°$ for HMGB (Box A + B) protein binding (9). The effect of HMGB binding on the flexibility of dsDNA was also previously studied in optical tweezers experiments (1,10). It was found that dsDNA force–extension curves were strongly altered by the presence of HMGB proteins. In the presence of several different HMGB proteins, the shape of the force–extension curves at low force indicated that the DNA persistence length was significantly reduced relative to that observed in the absence of protein. The change in persistence length as a function of protein concentration was used to determine protein equilibrium association constants and the average protein-induced DNA bending angle. The model used to determine the average bending angle assumed that the bound protein induced a random, flexible hinge (1,10). However, no direct information about the flexibility of

*To whom correspondence should be addressed. Tel: +1 617 373 2917; Fax: +1 617 373 2943; Email: n.israeloff@neu.edu
Correspondence may also be addressed to Mark C. Williams. Tel: +1 617 373 7323; Fax: +1 617 373 2943; Email: mark@neu.edu

the protein-bound site or distribution of angles could be obtained. For HU protein–DNA complexes, analysis of X-ray co-crystal structures indicated a fixed bend angle for a given structure, with a relatively narrow range of different angles observed in different structures. In contrast, atomic force microscopy (11–13) (AFM) studies of HU DNA-binding sites found a nearly flat distribution of bend angles, which provided strong evidence that protein binding formed a flexible hinge in that case (7).

In order to determine whether or not a flexible hinge mechanism for protein-enhanced DNA flexibility is broadly applicable, we now examine the distribution of bend angles for one and two box HMGB proteins. AFM allows us to directly observe protein-bound DNA structures (14–17), providing a complement to indirect measurement of DNA flexibility using optical or magnetic tweezers (1,7,18). A disadvantage of AFM is that 3D protein–DNA complexes must be deposited onto a 2D substrate, typically mica. However, with proper preparation, substrate effects on properties such as persistence length have been successfully modeled and minimized. When depositing dsDNA or protein–DNA complexes onto a mica surface, the result of the deposition depends on the nature and the strength of the molecule–surface interactions. Bustamante *et al.* (14) and Rivetti *et al.* (19) proposed that there exist two extremes in this process: equilibration and kinetic trapping. Equilibration occurs if the molecules can approach the substrate and establish an equilibrium conformation on the mica surface during the deposition process. On the other hand, if kinetic trapping occurs, parts of the dsDNA or protein–DNA complex adhere to the mica surface on contact, thereby becoming trapped at these sites.

If 2D equilibration occurs, it has been found that imaged molecules display persistence lengths quite close to those found in three dimensions in solution (19,20), suggesting that molecular flexibility and local bend angles are negligibly affected by substrate effects. Whether equilibration occurs is determined by the characteristic time $t$, required by the molecules to equilibrate on the wet mica surface relative to the deposition time before drying of the solvent. The characteristic time can be written as:

$$t = \frac{t_0}{1 - f_b\left[1 - \exp\left(-\frac{\Delta G_{bind}}{k_b T}\right)\right]} \quad \mathbf{1}$$

Here $f_b$ is fraction of the monomers of the dsDNA polymers interacting with positively charged ion-binding sites on the mica surface; $\triangle G_{\mathrm{bind}}$ is the binding energy of the molecule to each surface site; $k_B$ is the Boltzmann constant, $T$ is the deposition temperature, and $t_0$ is the characteristic time for the dsDNA polymer to access its equilibrium configurations with free diffusion on the 2D surface. Bustamante and Rivetti, (19,20) also pointed out that typically, for 5994 base-pair (bp) dsDNA fragments, the characteristic time, $t$, is about 5 min and for shorter dsDNA fragments, as little as 1 min is required to attain equilibrium. For the pBR322 dsDNA fragments (4361 bp) studied here, the characteristic time $t$ should be well under 5 min, much less than the deposition time used in sample preparation. Therefore, the results presented in this study reflect the characteristics of equilibrium protein–DNA structures. Our studies of equilibrium DNA–protein complexes show for the first time that the behavior of HMGB proteins is intermediate between that expected for a flexible hinge or static kink interaction mechanism.

## MATERIALS AND METHODS

Freshly cleaved mica is used as the substrate to deposit dsDNA and protein–DNA complexes. Because freshly cleaved mica is negatively charged (20,21), $Mg^{2+}$, a divalent cation, was used in the deposition buffer to promote the adhesion of negatively charged DNA to the mica surface and prevent (18) binding of HMGB proteins (21,22). Isolated plasmid pBR322 (Fermentas) was linearized by digestion with *Pvu*II (Fermentas) followed by phenol extraction. The DNA was diluted with 10 mM Tris–HCl (pH 8.0), 5 mM $MgCl_2$ to 0.11 nM to avoid aggregation (23). Sample deposition involved the following steps: (i) muscovite mica (Ted Pella Inc.) was cleaved and washed with buffer containing 10 mM Tris–HCl pH 8.0, 5 mM $MgCl_2$. (ii) The sample was air dried, rinsed with 5 ml distilled water and air dried again. (iii) To collect images of bare DNA, a volume of 7 µl of the DNA solution (0.11 nM) was deposited on the mica surface for 10 min. (iv) The surface was rinsed with 5 ml distilled water and then air dried for 10–15 min, after which excess water was removed by careful blotting. Attempts at drying with an air stream produced elongated, non-equilibrated DNA, likely due to hydrodynamic forces. Samples were then imaged within 48 h.

To collect images of protein bound to DNA, HMGB2 (Box A) and HMGB1 (Box A + B) proteins were purified as described elsewhere (1) and were incubated with dsDNA before deposition. Optimal samples for imaging and analysis required moderate concentrations of both protein and dsDNA. A volume of 1.3 µl protein solution [20 nM HMGB2 (Box A) or HMGB1 (Box A + B)] and 7 µl of 0.11 nM DNA were combined.. Thus the sample consists of 0.09 nM DNA and 3.1 nM of either HMGB2 (Box A) or HMGB1 (Box A + B). The binding sizes for HMGB2 (Box A) and HMGB1 (Box A + B) proteins may be estimated to be 7 bp and ~18 bp, from previous studies (8,9,24). Therefore, the ratio of binding sites on the dsDNA to protein molecules is 18:1 and 7:1 respectively (nearly 1 protein for every 120 bp). This low protein/DNA concentration ratio allows enough dsDNA-binding sites while minimizing protein self-aggregation.

A Pico-Plus scanning probe microscope (SPM; Agilent Technology) was employed. The SPM was operated in tapping or intermittent contact mode in air. Tapping mode has been used widely for imaging soft biological samples. In this mode, the cantilever is driven at a fixed frequency (near its resonance frequency) as it scans the sample. The tip is allowed to make transient contact with the sample surface at the bottom of the oscillation, which reduces its oscillation amplitude. The amplitude is used as a height feedback control parameter. The height,

controlled by a piezo-crystal voltage, is extracted during scanning to form topography images. In addition, the phase of the oscillations is also used to form images. The resolution in tapping mode can be nearly as high as in contact mode, which is much more damaging to soft samples. Background cantilever thermal noise is inversely proportional to the resonance frequency (25), and a cantilever with higher resonance frequency allows for a faster scanning rate. Polymer surfaces become stiffer at higher frequencies, further reducing sample damage when using a high resonant frequency cantilever. Thus, cantilevers with the highest resonant frequency are preferable. Budget Sensors 300Al reflex silicon AFM tips were employed (resonance frequency ~300 kHz; spring constant ~40 N/m). Tips typically have ~10 nm radius of curvature, limiting lateral imaging resolution to ~15 nm under the best conditions. The scan range was either 2 μm × 2 μm or 1 μm × 1 μm at 512 × 512 pixels. The scan rate was typically 2 Hz. Both topography and phase images were analyzed. DNA contours were traced semi-automatically using ImageJ software (26) from NIH with the NeuronJ plug-in (27). The tracing step size varied from 1 to 10 pixels. The DNA bend angle was measured at the protein-binding site using National Instruments Vision Assistant 7.0 software.

## RESULTS

Bare linearized dsDNA from plasmid pBR322 (4361 bp) was initially imaged (Figure 1). The distribution of contour lengths obtained from 40 molecules by image tracing (Figure 2a) had a mean of 1.48 μm, and SD σ = 0.11 μm, giving 0.34 ± 0.03 nm per bp, which agrees very well with the theoretical value of 0.34 nm per bp in B-form dsDNA (28). The local DNA bend angle is defined as the angle between the pair of adjacent line segments formed with three neighboring points along the contour, as shown in Figure 1b. Bend angles were measured for points at 10 nm intervals on the bare DNA molecules. The distribution of local bend angles was Gaussian-like (29), with a mean of 0° and σ ~22° (Figure 2b). However, resolution effects give an apparent width of DNA strands of approximately 15 nm, which causes measurement error in the angle data, particularly for small segment sizes. The image tracing algorithm affects this error somewhat, hence the error was estimated from the angle variance in visually straight sections of DNA. We estimated the angle error to be $\sigma' \sim 8^\circ$ for 10 nm segments. Therefore, the intrinsic DNA bend angle distribution should have width: $\sigma_0 = \sqrt{\sigma^2 - \sigma'^2} \sim 20.5^\circ$. For smaller segment sizes the angle error increases, as will be shown in the analysis of persistence length discussed below.

In order to estimate the DNA persistence length, the mean-squared end-to-end distance, $R^2$, was measured for individual dsDNA strands. Because dsDNA is a semi-flexible polymer (30,31) the Worm-Like Chain (WLC) model (32,33) can be used. With the assumption of equilibration, we used the 2D WLC model to determine the persistence length (19):

$$\langle R^2 \rangle = 4pL\left[1 - \frac{2p}{L}\left(1 - e^{-L/2p}\right)\right] \quad \mathbf{2}$$

where $<R^2>$ is the mean-squared end-to-end distance, and $p$ and $L$ are the polymer persistence length and contour length, respectively. The mean-squared end-to-end distance $<R^2>$ was found to be $0.32 \pm 0.3\ \mu m^2$. Using Equation (2), we find the persistence length is 57 ± 6 nm (168 ± 18 bp). This agrees very well with Rivetti's result (19), which gives 56 nm using the WLC model at this contour length, and is consistent with values found in solution.

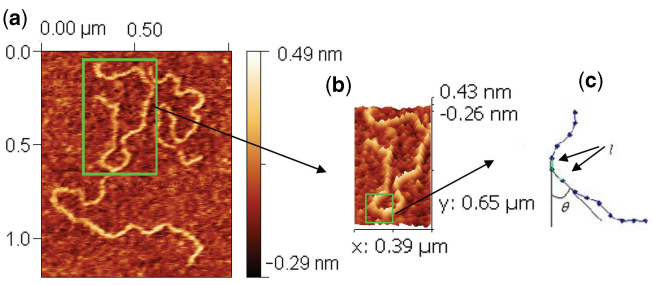


**Figure 1.** (**a**) 1 μm × 1.2 μm image of bare pBR322 dsDNA (contour length 1.5 μm). (**b**) 3D view of a single dsDNA molecule from (a). (**c**) Diagram showing local DNA bend angle calculation based on the angle between two adjacent line segments drawn between three adjacent points (step size l0 nm) along the contour.

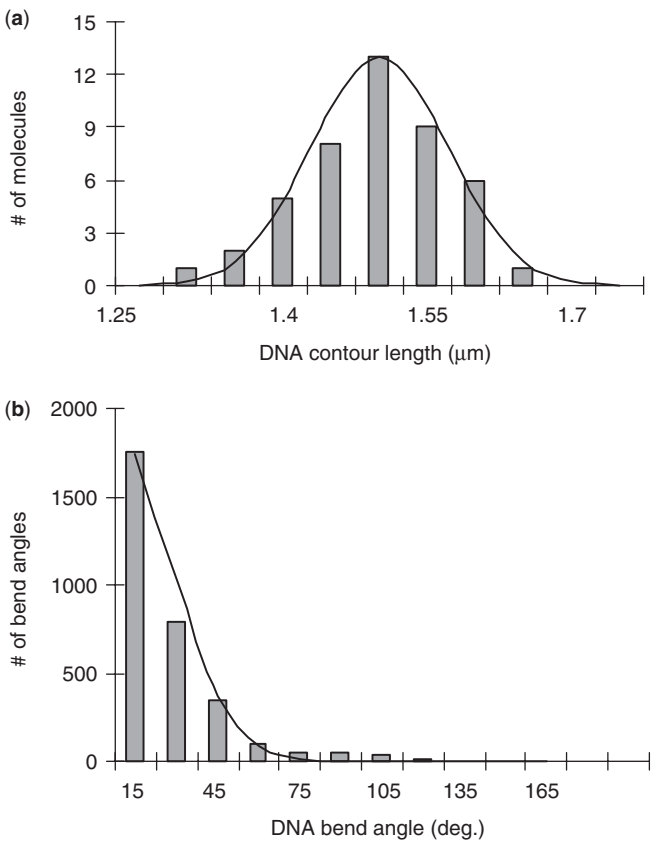


**Figure 2.** (**a**) The distribution of bare dsDNA contour lengths and its Gaussian fit. (**b**) The local bend angle distribution for bare dsDNA (segment step size 10 nm) and Gaussian fit.

We used a second method to estimate the persistence length of the bare dsDNA, which involved measuring the local DNA angle distribution. This method was first proposed by Landau and Lifshitz in 1958 (34). More recently, Rivetti *et al.* (19) and Abels *et al.* (35) deduced persistence length using a similar approach. By tracing the dsDNA contours, we calculated the local bend angle, $\theta$, of two consecutive segments at different step size $l$. Using the probability distribution function for the WLC model in two dimensions it can be shown that:

$$\langle \cos(\theta) \rangle = e^{-l/2p} \quad \mathbf{3}$$

Equation (3) can be transformed to Equation (4) by taking the natural logarithm on both sides:

$$-\ln(<\cos\theta>) = \frac{l}{2p} \quad \mathbf{4}$$

From a linear fit of this equation to the data, the slope $1/2p$, is extracted. The equation should only be valid up to $l \sim p$, and angle measurement errors are significant at small $l$, thus a good linear fit is expected only for intermediate values (19,36). Step sizes of 24 nm $< l <$ 66 nm were found to be optimal for determining $p$ (Figure 3). The persistence length obtained by this method was $p = 49.5 \pm 3.5$ nm, which agrees, within error, with the value found by the end-to-end distance method, and with 45–50 nm expected from solution studies (37). This illustrates the near equivalence of locally measured and globally measured polymer properties. In fact, the locally measured value should be more reliable than the end-to-end distance method because the choice of a limited step size range avoids excluded volume effects that can occur for longer polymers (19,36).

Surface effects must also be considered when analyzing protein-induced DNA bend angles. Bustamante *et al.* and Rivetti *et al.* (19,20) pointed out that the analysis is reliable only if the deposition process itself does not affect the conformation of the protein-induced DNA complexes. Under equilibration conditions, the protein–DNA-binding free energies are typically 15–30 times larger than the DNA-surface-binding energies (which are of order of $k_BT$). Therefore, DNA should attain equilibrium surface conformations via thermal energy without altering the protein-induced DNA bend angles. Alternatively, for kinetic trapping conditions, as discussed above, the surface binding may be strong enough to alter the protein-induced DNA complex conformation, including protein-induced DNA bend angles. Thus, bend angle analysis is only meaningful when conditions are favorable for equilibration, as was the case for the samples studied here.

Figure 4 shows images of DNA with bound HMGB proteins. As can be seen in the height profile (Figure 4b), the protein–DNA complexes project higher

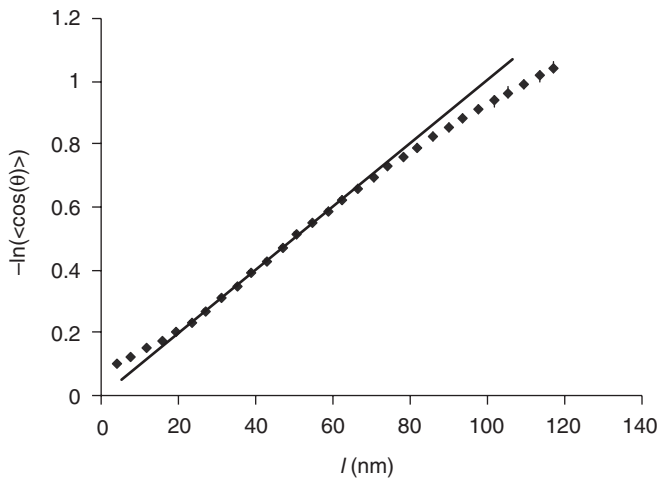


**Figure 3.** Local DNA bend angle versus segment step size. A linear fit is shown for the intermediate range of step sizes (from 24 to 66 nm).

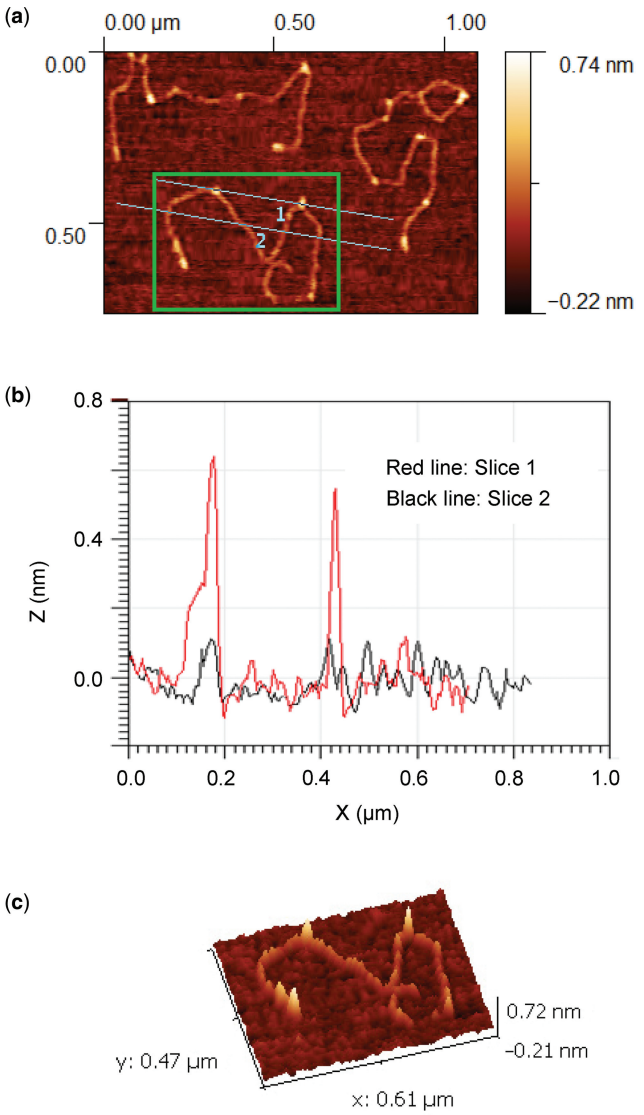


**Figure 4.** (**a**) Images for three individual HMGB protein–DNA complexes. (**b**) Height information is provided for the two lines shown on the image: slice 1 crosses the only the bare dsDNA. The peak height is no more than 0.1 nm. Slice 2 crosses two bound HMGB proteins and the peak heights are more than 0.55 nm. (**c**) 3D view of the single DNA molecule selected from (a) showing bound proteins as spikes.

from the mica surface than bare DNA, typically by ~0.5 nm. These bound proteins thus appear as light colored spots in the images. Figure 4c provides a 3D image rendering, clearly showing the bound proteins as relatively higher spikes. Thus, bound HMGB proteins were identified visually by this significant height difference. Protein-induced DNA bend angles could then be measured at the protein-binding sites, with a measurement error of ~5°, and the distribution of these angles was determined (Figure 5). The distribution shows an average induced DNA bend angle of 78° with a SD of 23° for HMGB (Box A) protein and for HMGB (Box A + B) an average DNA bend angle of 67° with a SD of 21° was found. The error in the average bend angle measurement was ±1.3°.

A second method, based on the global average flexibility, was also used to obtain the average local bend angle. Since the structure of a protein–DNA complex is heterogeneous, the WLC model (Equation 3) (13) for a homogeneous structure is no longer valid. We may quantify the relationship between the persistence length, $p$, of the bare DNA, the end-to-end distance of the protein-induced DNA complexes, $<R^2>$, and the protein-induced bending angle, $\beta$, by using a model based on the WLC model but with intrinsic bends, as developed by Rivetti *et al.* (38) for the 3D case. In that model, the distribution of local protein-induced bend angles and the persistence length, $p$, for bare DNA are known inputs. The average $R^2$ is then calculated. We have adapted this approach and derived a relation for two dimensions. Using the average induced protein-site bend angle, $\beta$, the average number of bound proteins, $N$, and the bare DNA persistence length, $p$, the average $R^2$ can be found (see Supplementary Data for derivation):

$$\left\langle R_\beta^2 \right\rangle \approx 4pL\left(1 - \frac{2pN}{L}(1 - < \cos\beta >)\right) \quad \mathbf{5}$$

We counted the number of proteins bound to each individual dsDNA molecule. The distributions of $N$ for the two proteins are shown in Figure 6. The average number of proteins bound per DNA molecule under these binding conditions is three for HMGB2 (Box A) and four for HMGB1 (Box A + B). A Gaussian fit gave $\sigma \approx 1$ for both cases. It is then possible to apply the measured $<R^2>$ and Equation (5) to calculate the

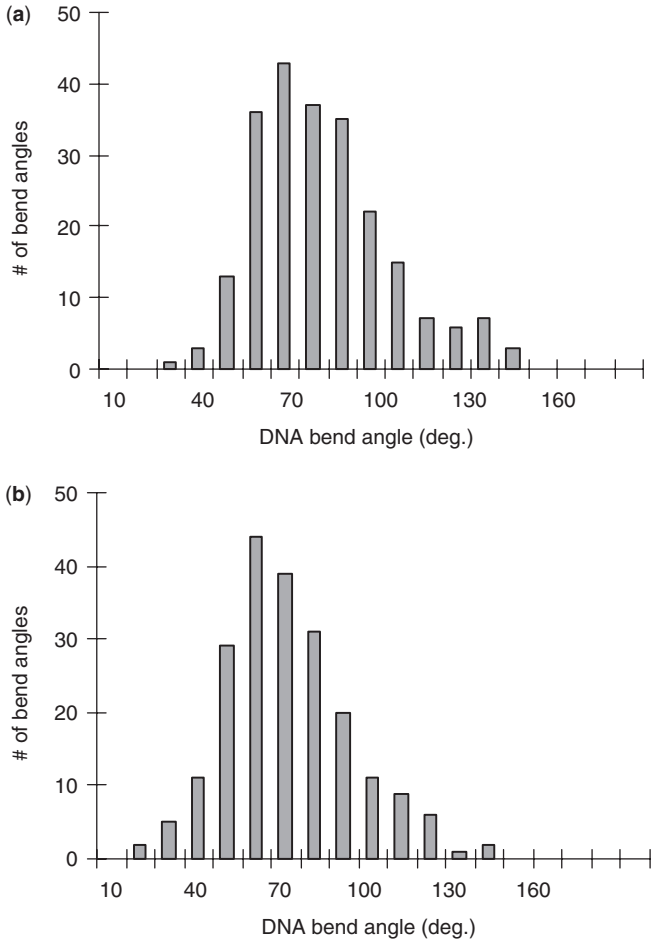


**Figure 5.** Distribution of protein-site bend angles for (**a**) HMGB (Box A) and (**b**) HMGB (Box A + B). The distribution shows an average induced DNA bend angle of 78° with a SD of 23° for HMGB (Box A) protein. HMGB (Box A + B) induces an average DNA bend angle of 67° with a SD of 21°.

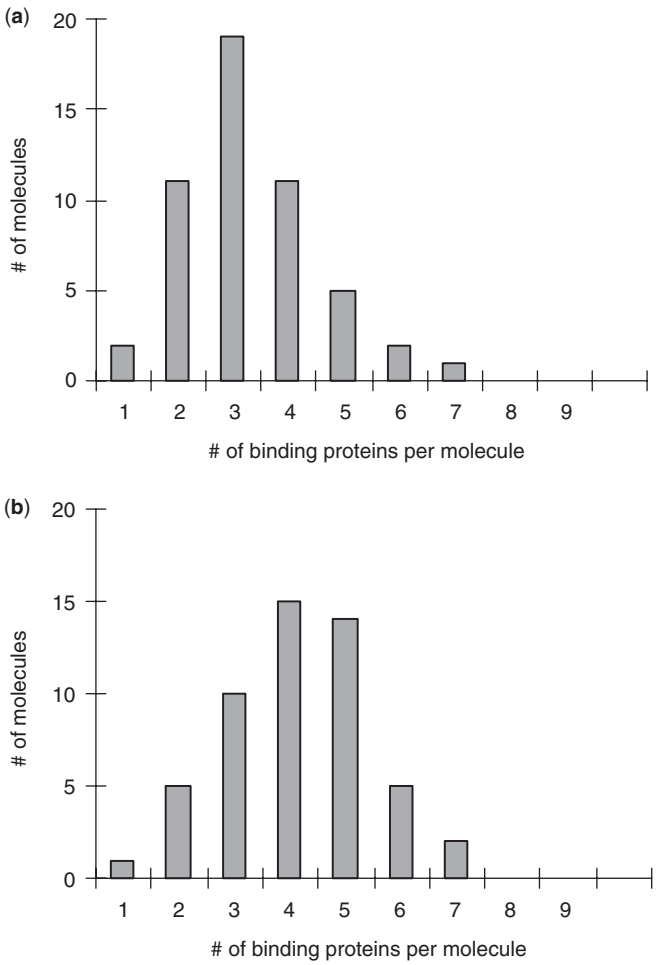


**Figure 6.** Distribution of the number of binding proteins per dsDNA molecule for (**a**) HMGB2 (Box A) and (**b**) HMGB1 (Box A + B).

average bend angle. For the HMGB2 (Box A) protein–DNA complexes, $R^2 = 0.27 \pm 0.04\,\mu m^2$ and for the HMGB1 (Box A + B) protein–DNA complexes, $R^2 = 0.26 \pm 0.05\,\mu m^2$. By this method the mean protein-site DNA bend angle, $<\beta>$, was found to be $82 \pm 8^\circ$ and $74 \pm 16^\circ$ for HMGB2 (Box A) and HMGB1 (Box A + B), respectively.

## DISCUSSION

In this study, bare DNA was imaged using AFM. DNA flexibility was then characterized through analysis of the DNA persistence length using two methods, one based on end-to-end distances and the other on locally measured bend-angles. Both methods used the 2D WLC model. The agreement between persistence lengths determined from the two methods (and also with bulk solution-based measurements) validated the approach and its assumptions. These results show that the molecules under study were well-equilibrated on the mica substrate and that substrate effects on local bend angles were weak.

For HMGB proteins bound to DNA, induced DNA bend angles were measured at the protein-binding site directly from the scanned images. Bend angles had moderately broad distributions that were much narrower than those found for HU binding (7). The mean bend angles obtained by this method were $78^\circ \pm 1.3^\circ$ for HMGB2 (Box A) and $67^\circ \pm 1.3^\circ$ for HMGB1 (Box A + B). We also used a variation of the WLC model to infer the mean protein-induced bend angle from measurement of a global property: end-to-end distances. This approach gave $82 \pm 8^\circ$ for HMGB2 (Box A) and $74 \pm 16^\circ$ for HMGB1 (Box A + B), consistent with the locally-measured mean angles. The distributions of the protein-induced locally measured bend angles were found to be moderately tight, with SDs of $23^\circ$ and $21^\circ$, respectively. These distributions are not consistent with a purely flexible-hinge model, in which there is no preferred bending angle, nor with a purely static kink model, in which each protein induces an identical fixed DNA bend angle. If bend angles varied significantly with local DNA sequence, this could broaden the distribution even if individual sites were static kinks of fixed angle (39). However, HMGB proteins are believed to bind sequence non-specifically, although it is possible that there may be a weak preference for certain AT-rich regions due to intrinsic DNA curvature (40,41). In any case, sequence neutral mechanisms for non-specific binding in HMG proteins suggest that bend angles are determined by the structure of the protein, which changes little on binding to DNA (8).

It is interesting to compare these results with those found in single-molecule DNA stretching experiments (1,10) where force–distance curves were measured versus protein concentration. Persistence lengths were derived from fits to a 3D WLC model. The protein-induced bend angle was then inferred from the persistence length in the fully saturated limit. The DNA bend angle estimates were $99^\circ \pm 9^\circ$ for HMGB2 (Box A) and $77^\circ \pm 7^\circ$ for HMGB1 (Box A + B). These values are quite close (given the assumptions made) but slightly larger than the values found here (Table 1). Significantly, in both measurements and the estimates from crystallography, the single box protein produces a larger bend angle. This is attributed to out-of-phase bending by the double-box protein. One difference between the optical tweezers analysis and the present experiments may arise from saturation effects on the local bend angle. With the AFM, we cannot easily measure local bend angles at high-protein concentration because of depletion and aggregation effects.

**Table 1.** Average DNA bend angles induced by HMGB proteins based on different experimental methods

| Method | HMGB2 (Box A) | HMGB1 (Box A + B) |
|---|---|---|
| X ray crystallography | $\sim 111^\circ$ (8)[a] | $101.5 \pm 9.1^\circ$ (9)[b] |
| Optical tweezers | $99 \pm 9^\circ$ (1) | $77 \pm 7^\circ$ (1) |
| AFM $<R^2>$ | $82 \pm 8^\circ$[c] | $74 \pm 16^\circ$[c] |
| AFM local angle | $78 \pm 1.3^\circ$ ($\sigma = 23^\circ$)[d] | $67 \pm 1.3^\circ$ ($\sigma = 21^\circ$)[d] |

[a]Crystallography data is from the *Drosophila melanogaster* single box HMGB protein HMG-D (protein databank entry 1QRV).
[b]To obtain the crystal structure of a two box protein, the authors replaced HMGB1 box A with the transcription factor SRY (protein databank entry 2GZK).
[c]$<R^2>$ is end-to-end distance method analyzed with Equation (5).
[d]Average angle data and the distribution width ($\sigma$) from Figure 5.

It is somewhat surprising that the present AFM results do not support the flexible hinge model, in contrast to results reported recently for the *E. coli* HU protein. HU is also a non-specific DNA binding protein that is believed to play a role in *E. coli* analogous to that of the HMGB proteins in eukaryotic systems. However, it should be noted that AFM imaging of HU was performed under kinetic trapping conditions (7), which may have resulted in an altered distribution of bend angles. Bustamante *et al.* have argued (14) that structural information obtained from AFM will only be reliable for equilibrated samples. On the other hand, it is not obvious how kinetic trapping conditions would result in such a broad distribution of binding angles. One mechanism for broadening the distribution relative to that present in solution would be the presence of strong non-uniform surface–DNA or surface–protein interactions. However, if the protein stays bound to the DNA under these conditions, then there must be significant flexibility to the protein–DNA interaction. Such a mechanism could also apply to our HMGB data, but is less likely for a surface coated with magnesium than one coated with cations of higher valence, such as the poly-lysine used in the HU study. The authors of the HU study also did a control experiment with another protein and showed a narrower distribution of angles in that case. It is also important to note that the structure and DNA bending mechanism of HU is entirely different from the HMGB family of proteins (9,42), and HU appears to have multiple DNA-binding modes (43). Based on these considerations, it is possible that the prokaryotic HU proteins interact with DNA through a different mechanism than eukaryotic HMGB proteins.

While the mechanism for enhancing DNA flexibility may differ for HU and HMGB proteins, they both achieve the same result—a significant enhancement of overall

apparent DNA flexibility. The result is interesting in light of recent single molecule studies, which detected a significant increase in flexibility for single DNA molecules, but which also showed that HMGB proteins failed to dissociate from DNA under certain solution conditions (10). Rapid dissociation and reassociation from DNA is required for a static kink model to effectively alter DNA flexibility on average. Therefore, HMGB proteins appear to enhance DNA flexibility by mechanisms that combine the static kink model, in which proteins bind to DNA transiently, inducing equal bends at random locations on the molecule, and by introducing some local DNA flexibility at the binding site. Our results also show that two-box HMGB1 (Box A + B) proteins are not more effective at bending DNA or increasing DNA flexibility. This is consistent with the suggestion made by McCauley *et al.* (1), in which an ensemble of double HMGB box proteins at fixed concentration would be more effective at increasing DNA flexibility due to the higher equilibrium DNA-binding affinity of double versus single box proteins, rather than due to a greater induced DNA bending angle.

## SUPPLEMENTARY DATA

Supplementary Data are available at NAR Online.

## ACKNOWLEDGEMENTS

We thank Dattatri Nagesha for technical assistance and Sri Sridhar and the NU Nanomedicine IGERT for use of the AFM.

## FUNDING

The work was supported by National Institutes of Health grants (GM075965 to L.J.M. and GM072462 to M.C.W.); National Science Foundation grants (MCB 0744456 to M.C.W and DMR-0606090 to N.E.I.); NIH and NCI IGERT grant (DGE-0504331); and the Mayo Clinic College of Medicine. Funding for open access charge: National Institutes of Health (GM075965).

*Conflict of interest statement*. None declared.

## REFERENCES

1. McCauley,M.J., Zimmerman,J., Maher,L.J. III and Williams,M.C. (2007) HMGB binding to DNA: single and double box motifs. *J. Mol. Biol.*, **374**, 993–1004.
2. Bustin,M. (1999) Regulation of DNA-dependent activities by the functional motifs of the high-mobility-group chromosomal proteins. *Mol. Cell. Biol.*, **19**, 5237–5246.
3. Bianchi,M.E. and Beltrame,M. (2000) Upwardly mobile proteins. Workshop: the role of HMG proteins in chromatin structure, gene expression and neoplasia. *EMBO Rep.*, **1**, 109–114.
4. Agresti,A. and Bianchi,M.E. (2003) HMGB proteins and gene expression. *Curr. Opin. Genet. Dev.*, **13**, 170–178.
5. Ross,E.D., Hardwidge,P.R. and Maher,L.J. III (2001) HMG proteins and DNA flexibility in transcription activation. *Mol. Cell. Biol.*, **21**, 6598–6605.
6. Travers,A.A., Ner,S.S. and Churchill,M.E. (1994) DNA chaperones: a solution to a persistence problem? *Cell*, **77**, 167–169.
7. van Noort,J., Verbrugge,S., Goosen,N., Dekker,C. and Dame,R.T. (2004) Dual architectural roles of HU: formation of flexible hinges and rigid filaments. *Proc. Natl Acad. Sci. USA*, **101**, 6969–6974.
8. Murphy,F.V. IV, Sweet,R.M. and Churchill,M.E.A. (1999) The structure of a chromosomal high mobility group protein–DNA complex reveals sequence-neutral mechanisms important for non-sequence-specific DNA recognition. *EMBO J.*, **18**, 6610–6618.
9. Stott,K., Tang,G.S.F., Lee,K.-B. and Thomas,J.O. (2006) Structure of a complex of tandem hmg boxes and DNA. *J. Mol. Biol.*, **360**, 90–104.
10. McCauley,M., Hardwidge,P.R., Maher,L.J. III and Williams,M.C. (2005) Dual binding modes for an HMG domain from human HMGB2 on DNA. *Biophys. J.*, **89**, 353–364.
11. Bustamante,C., Marko,J.F., Siggia,E.D. and Smith,S. (1994) Entropic elasticity of lambda-phage DNA. *Science*, **265**, 1599–1600.
12. Bustamante,C. and Keller,D. (1995) Scanning force microscopy in biology. *Phys. Today*, **48**, 32–38.
13. Hansma,H.G. (2001) Surface Biology of DNA by Atomic Force Microscopy. *Annu. Rev. Phys. Chem.*, **52**, 71–92.
14. Bustamante,C. and Rivetti,C. (1996) Visualizing protein-nucleic acid interactions on a large scale with the scanning force microscope. *Annu. Rev. Biophys. Biomol. Struct.*, **25**, 395–429.
15. Seong,G.H., Kobatake,E., Miura,K., Nakazawa,A. and Aizawa,M. (2002) Direct atomic force microscopy visualization of integration host factor induced DNA bending structure of the promoter regulatory region on the Pseudomonas TOL plasmid. *Biochem. Biophys. Res. Commun.*, **291**, 361–366.
16. Janicijevic,A., Sugasawa,K., Shimizu,Y., Hanaoka,F., Wijgers,N., Djurica,M., Hoeijmakers,J.H. and wyman,C. (2003) DNA bending by the human damage recognition complexes XPC-HR23B. *DNA Repair*, **2**, 325–336.
17. Mysiak,M.E., Bleijenberg,M.H., Wyman,C., Holthuizen,P.E. and Van Der Vliet,P.C. (2004) Bending of adenovirus origin DNA by nuclear factor I as shown by scanning force microscopy is required for optimal DNA replication. *J. Virol.*, **78**, 1928–1935.
18. Mihailovic,A., Vladescu,I., McCauley,M., Ly,E., Williams,M.C., Spain,E.M. and Nunez,M.E. (2006) Exploring the interaction of ruthenium(II) polypyridyl complexes with DNA using single-molecule techniques. *Langmuir*, **22**, 4699–4709.
19. Rivetti,C., Guthold,M. and Bustamante,C. (1996) Scanning force microscopy of DNA deposited onto mica: equilibration versus kinetic trapping studied by statistical polymer chain analysis. *J. Mol. Biol.*, **264**, 919–932.
20. Bustamante,C. and Rivetti,C. (1996) Visualizing protein-nucleic acid interactions on a large scale with the scanning force microscope. *Annu. Rev. Biophys. Biomol. Struct.*, **25**, 395–429.
21. Zheng,J., Li,Z., Wu,A. and Zhou,H. (2003) AFM studies of DNA structures on mica in the presence of alkaline earth metal ions. *Biophys. Chem.*, **104**, 37–43.
22. Thomson,N.H., Kasas,S., Smith,B.L., Hansma,H.G. and Hansma,P.K. (1996) Reversible binding of DNA to mica for AFM imaging. *Langmuir*, **12**, 5905–5908.
23. Allen,M.J., Bradbury,E.M. and Balhorn,R. (1997) AFM analysis of DNA-protamine complexes bound to mica. *Nucleic Acids Res.*, **25**, 2221–2226.
24. Churchill,M.E., Changela,A., Dow,L.K. and Krieg,A.J. (1999) Interactions of high mobility group box proteins with DNA and chromatin. *Meth. Enzymol.*, **304**, 99–103.
25. Albrecht,T.R., Grutter,P., Horne,D. and Rugar,D. (1991) Frequency modulation detection using high-Q cantilevers for enhanced force microscope sensitivity. *J. Appl. Phys.*, **69**, 668–673.
26. Abràmoff,M.D., Magalhães,P.J. and Ram,S.J. (2004) Image processing with image. *J. Biophot. Int.*, **11**, 36–42.
27. Meijering,E., Jacob,M., Sarria,J.-C.F., Steiner,P., Hirling,H. and Unser,M. (2004) Design and validation of a tool for neurite tracing and analysis in fluorescence microscopy images. *Cytometry*, **58A**, 167–176.
28. Watson,J.D. and Crick,F. (1953) Molecular structure of nucleic acids: a structure for deoxyribose nucleic acid. *Nature*, **171**, 737–738.
29. Rivetti,C. and Codeluppi,S. (2001) Accurate length determination of DNA molecules visualized by atomic force microscopy: evidence for a partial B- to A-form transistion on mica. *Ultramicroscopy*, **87**, 55–66.

30. Kratky,O. and Porod,G. (1949) Rontgenuntersuchung aufgeloster fademolekule. *Recueil*, **68**, 1106–1122.
31. Schellman,J.A. (1974) Flexibility of DNA. *Biopolymers*, **13**, 217–226.
32. Grosberg,A.Y. and Khokhlov,A.R. (1994) *Statistical Physics of Macromolecules*, API, Woodbury, NY.
33. Wiggins,P.A., van der Heijden,T., Moreno-Herrero,F., Spakowitz,A., Phillips,R., Widom,J., Dekker,C. and Nelson,P.C. (2006) High flexibility of DNA on short length scales probed by atomic force microscopy. *Nature Nanotech.*, **1**, 137–141.
34. Landau,L.D. and Lifshitz,E.M. (1958) *Course of Theoretical Physics*, Pergamon, London.
35. Abels,J.A., Moreno-Herrero,F., van der Heijden,T., Dekker,C. and Dekker,N.H. (2005) Single-Molecule Measurements of the Persistence Length of double-stranded RNA. *Biophys. J.*, **88**, 2737–2744.
36. Joanicot,M. and Revet,B. (1987) DNA conformational studies from electron microscopy. I. Excluded volume effect and structure dimensionality. *Biopolymers*, **26**, 315–326.
37. Hagerman,P.J. (1988) Flexibility of DNA. *Annu. Rev. Biophys. Biophys. Chem.*, **17**, 265–286.
38. Rivetti,C., Walker,C. and Bustamante,C. (1998) Polymer chain statistics and conformational analysis of DNA molecules with bends or sections of different flexibility. *J. Mol. Biol.*, **280**, 41–59.
39. Erie,D.A., Yang,G., Schultz,H.C. and Bustamante,C. (1994) DNA bending by Cro protein in specific and nonspecific complexes: implications for protein site recognition and specificity. *Science*, **266**, 1562–1566.
40. Bustin,M. and Reeves,R. (1996) High-mobility-group chromosomal proteins: architectural components that facilitate chromatin function. *Prog. Nucleic Acid Res. Mol. Biol.*, **54**, 35–100.
41. Grosschedl,R., Giese,K. and Pagel,J. (1994) HMG domain proteins: architectural elements in the assembly of nucleoprotein structures. *Trends Genet.*, **10**, 94–100.
42. Rice,P.A., Yang,S., Mizuuchi,K. and Nash,H.A. (1996) Crystal structure of an IHF-DNA complex: a protein-induced DNA U-turn. *Cell*, **87**, 1295–1306.
43. Koh,J., Saecker,R.M. and Record,M.T. Jr. (2008) DNA binding mode transitions of Escherichia coli HU(alphabeta): evidence for formation of a bent DNA–protein complex on intact, linear duplex DNA. *J. Mol. Biol.*, **383**, 324–346.